Dynamic-polarization forces on fast ions and molecules moving over supported graphene

I. Radović, Lj. Hadžievski, and N. Bibić
VINČA Institute of Nuclear Sciences, P.O. Box 522, 11001 Belgrade, Serbia

Z. L. Mišković*
Department of Applied Mathematics, University of Waterloo, Waterloo, Ontario, Canada N2L 3G1
(Received 12 June 2007; published 4 October 2007)

We use a two-dimensional, two-fluid hydrodynamic model to describe the high-frequency plasmon excitations of the carbon valence electrons responding to fast ions and electric dipoles, which move parallel to a single sheet of graphene supported by an insulating substrate. We calculate the stopping and the image forces on ions and dipoles, as well as the dynamic torque on dipoles about their center of mass, resulting from the dynamic polarization of graphene. While the results for ions are similar to those obtained earlier for ion channeling through carbon nanotubes in dielectric media, the stopping and the image forces on dipoles show strong directional dependencies. The torque on point dipoles implies a strong alignment effect in the direction of motion at lower speeds, as well as a tendency of the dipole to "roll" over the graphene at high speeds.

DOI: 10.1103/PhysRevA.76.042901 PACS number(s): 79.20.Rf, 34.50.Bw, 34.50.Dy

I. INTRODUCTION

Renewed interest in the properties of two-dimensional (2D) electron systems is stimulated by recent discovery of graphene, a single sheet of carbon atoms forming hexagonal lattice, which exhibits electronic properties of a semimetal [1,2]. Besides being the fundamental building block of highly oriented pyrolytic graphite (HOPG), carbon nanotubes, and fullerene molecules, graphene is currently attracting a great deal of interest on its own right owing to its fascinating physical properties and a broad range of potential application areas [3], including the emerging field of plasmonics [4]. Namely, recent investigations of the low-energy collective electron excitations in graphene show that this material may be used as a basis for nanoelectronic devices operating in the terahertz range of frequencies owing to the peculiar behavior of the graphene π electrons as a 2D gas of massless Dirac fermions for the band energies up to a few eV [5–7].

On the other hand, interactions with external charged particles moving over graphene at speeds far greater than its Fermi velocity, are dominated by the collective electron excitations at the optical and ultraviolet frequencies, involving both π and σ electrons. Such processes are ubiquitous in the electron energy loss spectroscopy (EELS) of graphene-based materials [8–10], and can play an important role in ion scattering from the surface of such targets. For example, the directional effects in the interactions of heavy, energetic charges with highly oriented pyrolytic graphite (HOPG) have been recently studied in several contexts, including ion and molecule implantation in HOPG [11], ion channeling through HOPG [12], and secondary electron emission from HOPG induced by fast ions [13] and molecules [14]. In addition, studying scattering of fast ions from free and supported graphene under grazing incidence may open interesting parallels with the phenomena discovered in the scattering experiments on solid surfaces [15]. For example, one can speculate on the kinds of defect formation on graphene by analogy with the recent studies of nanostructures formed on crystal surfaces due to the impact of highly charged ions [16,17]. It is further interesting to note that, while the dynamic polarization effects in surface grazing scattering have been well understood for ionic projectiles [15,16], similar processes involving fast molecules have received attention only very recently [18] from the perspective of possible applications in the molecular transmission through nanocapillaries [19].

With a view of extending these studies of solid surfaces to graphene, we explore here the effects of dynamic polarization of graphene on forces acting on fast ions and polar molecules moving parallel to it. Specifically, we calculate the stopping force and the image force which, in the regime of high projectile speeds and large distances from graphene, respectively, describe the dissipation of the projectile's kinetic energy into plasmon excitations in graphene, and the conservative force attracting the projectile towards graphene. In addition, we calculate here for the first time the torque on polar molecules represented by an electric dipole, thus generalizing the discussion of the alignment effects for slow dimers moving in a homogeneous electron gas [20], for slow polar molecules on solid surfaces [21,22], and fast diclusters grazingly scattered from metal surfaces [23], to the case of fast molecules under grazing incidence upon graphene.

Given that such processes are dominated by the high-frequency plasmon excitations of all four valence electrons in graphene, we use here the 2D, two-fluid, semiclassical hydrodynamic model based on the jellium approximation for the positive ion charges in graphene [24–26]. It has been shown that treating the σ and π electrons as two interacting fluids provides a qualitatively correct account of the splitting of plasmon branches in the visible and uv ranges of frequencies in both fullerenes [25] and single-wall carbon nanotubes [26]. Although hydrodynamic models of the electron gas are generally considered to be of only limited quantitative value compared to, e.g., random phase approximation for the response of carbon nanotubes [27], they have proven to be

*zmiskovi@math.uwaterloo.ca

quite effective in the qualitative analysis of plasmon hybridization of relevance in the area of plasmonics [28]. Moreover, hydrodynamic models of plasmon excitations in nanostructures appear to be quite versatile in handling the boundary conditions due to the presence of a dielectric environment [29], as is often the case with graphene [8,30]. While the configuration of a graphene sheet supported by a substrate opens an interesting possibility of exciting novel plasmon modes in the case of metallic substrate [8,31], we limit ourselves here to the insulating substrate, such as SiO_2 lying underneath a single graphene sheet [30].

After outlining the theoretical model in the following section, we shall present and discuss the results for the stopping and image forces on point ions and point dipoles, as well as for the torque on point dipoles. Atomic units will be used throughout unless otherwise stated explicitly.

II. BASIC THEORY

We use a Cartesian coordinate system with $\mathbf{R}=\{\mathbf{r},z\}$ and assume that graphene occupies its xy plane with coordinates $\mathbf{r}=\{x;y\}$. Furthermore, a fast projectile is assumed to move parallel to the graphene in the upper half-space defined by $z>0$, while the planar surface of a substrate is assumed to be placed at distance h underneath the graphene. Thus, the substrate occupying the region $z\leqslant -h$ is assumed to be described by an abrupt jump in the dielectric constant from unity characterizing vacuum or air, to a (constant) value ϵ. In order to treat the effects of substrate on the dynamic response of graphene to external perturbation, we follow the method of Doerr and Yu [29,32] and assume that a polarization charge is induced on the substrate surface with the density per unit area $\sigma(\mathbf{r},t)$. Then, integrating Gauss' law for the total electric field $\boldsymbol{\nabla}\cdot\mathbf{E}=4\pi\sigma(\mathbf{r},t)\delta(z+h)$, gives the boundary condition for the total electric potential $\Phi(\mathbf{R},t)$ at the substrate surface,

$$\left.\frac{\partial\Phi}{\partial z}\right|_{z=-h+0} - \left.\frac{\partial\Phi}{\partial z}\right|_{z=-h-0} = -4\pi\sigma. \tag{1}$$

If there are no free charges on the substrate surface, one may integrate Gauss' law for the electric displacement field $\boldsymbol{\nabla}\cdot\mathbf{D}=0$, with $\mathbf{D}\equiv\epsilon(z)\mathbf{E}$, to obtain

$$\left.\frac{\partial\Phi}{\partial z}\right|_{z=-h+0} - \epsilon \left.\frac{\partial\Phi}{\partial z}\right|_{z=-h-0} = 0. \tag{2}$$

The key point in the method of Doerr and Yu [32] is to write the total electric potential Φ as the sum of the external perturbing potential Φ_e, the potential due to charge polarization on graphene Φ_g, and the potential due to the induced surface charge on the substrate Φ_s, so that

$$\Phi = \Phi_e + \Phi_g + \Phi_s. \tag{3}$$

Further, one can define Φ_s to satisfy the boundary condition

$$\left.\frac{\partial\Phi_s}{\partial z}\right|_{z=-h+0} - \left.\frac{\partial\Phi_s}{\partial z}\right|_{z=-h-0} = -4\pi\sigma, \tag{4}$$

by writing the solution of the Poisson's equation for the induced charge on substrate $\nabla^2\Phi_s=-4\pi\sigma(\mathbf{r},t)\delta(z+h)$, as

$$\Phi_s(\mathbf{R},t) = \int d^3\mathbf{R}' \frac{\sigma(\mathbf{r}',t)\delta(z'+h)}{\|\mathbf{R}-\mathbf{R}'\|}. \tag{5}$$

While this choice of Φ_s ensures that the total electric potential satisfies Eq. (1), the actual expression for σ (and hence Φ_s) will be obtained by applying Eq. (2).

It is convenient to introduce Fourier transform $\tilde{A}(\mathbf{k},z,\omega)$, with respect to time and coordinates in the xy plane, defined by

$$A(\mathbf{R},t) = \int \frac{d^2\mathbf{k}}{(2\pi)^2}\frac{d\omega}{2\pi} e^{i\mathbf{k}\cdot\mathbf{r}-i\omega t}\tilde{A}(\mathbf{k},z,\omega),$$

of an arbitrary function $A(\mathbf{R},t)\equiv A(\mathbf{r},z,t)$, with $\mathbf{k}=\{k_x,k_y\}$. Then, one obtains

$$\tilde{\Phi}_s(\mathbf{k},z,\omega) = \frac{2\pi}{k} e^{-k|z+h|}\tilde{\sigma}(\mathbf{k},\omega), \tag{6}$$

where $k=\sqrt{k_x^2+k_y^2}$ and $\tilde{\sigma}(\mathbf{k},\omega)$ is the Fourier transform of the polarization charge on the substrate surface. Similarly, if $n(\mathbf{r},t)$ is the perturbation of the number density per unit area of electrons in graphene, one obtains

$$\tilde{\Phi}_g(\mathbf{k},z,\omega) = -\frac{2\pi}{k} e^{-k|z|}\tilde{n}(\mathbf{k},\omega). \tag{7}$$

Next, we describe the σ and π electrons in graphene as two fluids occupying the xy plane and having the equilibrium number densities per unit area $n_\sigma^0\approx 0.321$ and $n_\pi^0\approx 0.107$, respectively. The perturbations of their densities $n_j(\mathbf{r},t)$ and their velocity fields $\mathbf{u}_j(\mathbf{r},t)$, with $j=\sigma,\pi$, satisfy the linearized continuity equation,

$$\frac{\partial n_j(\mathbf{r},t)}{\partial t} + n_j^0\boldsymbol{\nabla}_\mathbf{r}\cdot\mathbf{u}_j(\mathbf{r},t) = 0, \tag{8}$$

and the linearized momentum-balance equation,

$$\frac{\partial\mathbf{u}_j(\mathbf{r},t)}{\partial t} = \boldsymbol{\nabla}_\mathbf{r}\,\Phi(\mathbf{R},t)|_{z=0} - \frac{\alpha_j}{n_j^0}\boldsymbol{\nabla}_\mathbf{r} n_j(\mathbf{r},t) - \gamma_j\mathbf{u}_j(\mathbf{r},t). \tag{9}$$

Here, $\boldsymbol{\nabla}_\mathbf{r}$ is the component of the full gradient operator which differentiates in directions parallel to the xy plane. The first term on the right-hand side of Eq. (9) is the tangential force on an electron due to the total electric field at $z=0$. The second term describes the internal interactions in the electron fluids based on the Thomas-Fermi model [33,34], giving $\alpha_j=\pi n_j^0$. The last term in Eq. (9) represents the frictional force on an electron due to scattering on the positive charge background, with γ_j being the frictional coefficient which we take to be vanishingly small. Solving the fluid equations by means of the Fourier transform gives a relation between the total electron number density on graphene, $n=n_\sigma+n_\pi$, and the local value of the total potential at $z=0$ in the form

$$\tilde{n}(\mathbf{k},\omega) = \chi(k,\omega)\tilde{\Phi}(\mathbf{k},z=0,\omega), \tag{10}$$

where the polarization function of graphene in the two-fluid model is given by $\chi(k,\omega)=\chi_\sigma(k,\omega)+\chi_\pi(k,\omega)$ with

$$\chi_j(k,\omega) = \frac{n_j^0 k^2}{\alpha_j k^2 - \omega(\omega + i\gamma_j)} \quad \text{for } j = \sigma, \pi. \tag{11}$$

Using the relation (10) along with Eqs. (6) and (7) and the Fourier transforms of the boundary condition (2) and the decomposition of the total potential (3), one can obtain the induced densities $\tilde{n}$ and $\tilde{\sigma}$ in terms of the local value of the external potential $\tilde{\Phi}_e(\mathbf{k},z,\omega)$ at the graphene plane and its derivative perpendicular to the substrate surface. Since we are interested in values of the induced potential $\Phi_{\text{ind}}=\Phi_s+\Phi_g$, restricted to the region above graphene ($z>0$), its Fourier transform can be written as

$$\tilde{\Phi}^{>}_{\text{ind}}(\mathbf{k},z,\omega) = -\frac{2\pi}{k}e^{-kz}\frac{\chi\left(1-\frac{\epsilon-1}{\epsilon+1}e^{-2kh}\right)\tilde{\Phi}_e|_{z=0} + \frac{\epsilon-1}{\epsilon+1}\frac{e^{-kh}}{2\pi}\left.\frac{\partial\tilde{\Phi}_e}{\partial z}\right|_{z=-h}}{1+\frac{2\pi}{k}\chi\left(1-\frac{\epsilon-1}{\epsilon+1}e^{-2kh}\right)}. \tag{12}$$

We consider a projectile represented by a rigid distribution of charge with the volume density function $\hat{\rho}_{\text{ext}}(\mathbf{R})$, which moves parallel to the graphene at constant velocity $\mathbf{V}=\{\mathbf{v},0\}$ with $\mathbf{v}=\{v_x,v_y\}$, so that its density in the laboratory frame of reference can be written as $\rho_{\text{ext}}(\mathbf{R},t)\equiv\hat{\rho}_{\text{ext}}(\mathbf{R}-\mathbf{V}t)$. Therefore, the Fourier transform of the external potential can be expressed as

$$\tilde{\Phi}_e(\mathbf{k},z,\omega) = 2\pi\delta(\omega-\mathbf{k}\cdot\mathbf{v})\frac{2\pi}{k}\int d^3\mathbf{R}'e^{-i\mathbf{k}\cdot\mathbf{r}'-k|z-z'|}\hat{\rho}_{\text{ext}}(\mathbf{R}'). \tag{13}$$

Since in Eq. (12) we only need values of $\tilde{\Phi}_e(\mathbf{k},z,\omega)$ for $z\leq 0$, assuming that the external charge $\hat{\rho}_{\text{ext}}(\mathbf{R})$ is fully localized above the graphene plane allows us to write

$$\tilde{\Phi}^{<}_e(\mathbf{k},z,\omega) = 2\pi\delta(\omega-\mathbf{k}\cdot\mathbf{v})\frac{2\pi}{k}e^{kz}\mathcal{F}(\mathbf{k}), \tag{14}$$

with the structure factor of the external charge given by

$$\mathcal{F}(\mathbf{k}) = \int d^3\mathbf{R}\hat{\rho}_{\text{ext}}(\mathbf{R})f(\mathbf{R};\mathbf{k}), \tag{15}$$

where we have defined $f(\mathbf{R};\mathbf{k})\equiv e^{-i\mathbf{k}\cdot\mathbf{r}-kz}$.

The factor $\delta(\omega-\mathbf{k}\cdot\mathbf{v})$, appearing in Eqs. (13) and (14), will be carried into Eq. (12), implying that the induced potential is stationary in the moving frame of reference attached to the external charge distribution. Denoting this potential by $\hat{\Phi}_{\text{ind}}(\mathbf{R})$, we note that the induced potential in the laboratory frame is then $\Phi_{\text{ind}}(\mathbf{R},t)\equiv\hat{\Phi}_{\text{ind}}(\mathbf{R}-\mathbf{V}t)$. Taking this into account while inserting Eq. (14) into Eq. (12) and performing the inverse Fourier transform, one obtains

$$\hat{\Phi}^{>}_{\text{ind}}(\mathbf{R}) = \int\frac{d^2\mathbf{k}}{(2\pi)^2}f^*(\mathbf{R};\mathbf{k})\frac{2\pi}{k}\mathcal{F}(\mathbf{k})\left[\frac{1}{D(k,\mathbf{k}\cdot\mathbf{v})}-1\right], \tag{16}$$

where

$$D(k,\omega) = \Gamma(k) + \frac{2\pi}{k}\chi(k,\omega), \tag{17}$$

with the auxiliary function

$$\Gamma(k) \equiv \frac{\epsilon+1}{2}\frac{1+\coth(kh)}{\epsilon+\coth(kh)}, \tag{18}$$

quantifying the effects of the substrate on the response of graphene. One notices that, when $\epsilon=1$ or $kh\to+\infty$, $\Gamma(k)$ reaches its minimal value $\Gamma_{\text{min}}=1$ corresponding to a free-standing graphene layer, whereas its maximal value $\Gamma_{\text{max}}=(\epsilon+1)/2$ (for fixed ϵ) is reached for $kh\to 0$.

In passing, we note that, for $\epsilon=$const, the zeros of $D(k,\omega)$ give two plasmon branches with the dispersion relations defined by

$$\omega_\pm^2(k) = \frac{\omega_\pi^2(k)+\omega_\sigma^2(k)}{2} \pm \sqrt{\left[\frac{\omega_\pi^2(k)-\omega_\sigma^2(k)}{2}\right]^2+\left[\frac{2\pi k}{\Gamma(k)}\right]^2 n_\sigma^0 n_\pi^0}, \tag{19}$$

where

$$\omega_j^2(k) = \frac{2\pi k}{\Gamma(k)}n_j^0 + \alpha_j k^2 \quad \text{for } j=\sigma,\pi, \tag{20}$$

are the single-fluid plasmon dispersions for noninteracting σ and π electrons. One can show that the long wavelength limit of the low-frequency plasmon branch behaves quasiacoustically, with the dispersion relation $\omega_-(k)=v_a k$, where the "acoustic" speed $v_a=\sqrt{3\pi n_0/8}\approx 0.71$ ($n_0\approx 0.428$ being the surface density of valence electrons in graphene) is not affected by the presence of the substrate. On the other hand, the high-frequency plasmon branch exhibits typical 2D dispersion, $\omega_+(k)=\sqrt{4\pi n_0 k/(\epsilon+1)}$, which is suppressed by the factor $\sqrt{2/(\epsilon+1)}$ due to the presence of the substrate when compared to the free-graphene case.

One can use expression (16) to study the effects of dynamic polarization of graphene on the external charge. So, its self-energy $\mathcal{E}_{\text{self}}$, or the image potential is obtained as

$$\mathcal{E}_{\text{self}} \equiv \frac{1}{2}\int d^3\mathbf{R}\hat{\rho}_{\text{ext}}(\mathbf{R})\hat{\Phi}_{\text{ind}}(\mathbf{R}) = \frac{1}{2}\int \frac{d^2\mathbf{k}}{(2\pi)^2}\frac{2\pi}{k}|\mathcal{F}(\mathbf{k})|^2\left[\frac{1}{D(k,\mathbf{k}\cdot\mathbf{v})}-1\right], \quad (21)$$

whereas the dynamic polarization force $\mathbf{F}_{\text{ind}}$ on the external charge is obtained from the induced electric field in the moving frame $\hat{\mathbf{E}}_{\text{ind}}(\mathbf{R})=-\nabla\hat{\Phi}_{\text{ind}}(\mathbf{R})$, as

$$\mathbf{F}_{\text{ind}} \equiv \int d^3\mathbf{R}\hat{\rho}_{\text{ext}}(\mathbf{R})\hat{\mathbf{E}}_{\text{ind}}(\mathbf{R}) = \int \frac{d^2\mathbf{k}}{(2\pi)^2}(k\mathbf{e}_z - i\mathbf{k})\frac{2\pi}{k}|\mathcal{F}(\mathbf{k})|^2\left[\frac{1}{D(k,\mathbf{k}\cdot\mathbf{v})}-1\right], \quad (22)$$

where $\mathbf{e}_z$ is a unit vector in the direction of the z axis. We note that this force consists of a conservative part corresponding to the image force on the projectile F_i, which acts in the direction perpendicular to graphene, and a dissipative part, giving rise to the stopping force F_s, which acts in the direction opposing projectile's motion. Proceeding in a similar fashion, one can also define the torque $\boldsymbol{\tau}$ on the external charge distribution about some point $\mathbf{R}_0$ in the moving frame as [35]

$$\boldsymbol{\tau} \equiv \int d^3\mathbf{R}\hat{\rho}_{\text{ext}}(\mathbf{R})(\mathbf{R}-\mathbf{R}_0)\times\hat{\mathbf{E}}_{\text{ind}}(\mathbf{R}). \quad (23)$$

While the torque on a point charge centered at $\mathbf{R}_0=\mathbf{0}$ is clearly zero, a finite distribution of charges, like in polar molecules, may experience rotation about its center of mass, placed at $\mathbf{R}_0$, due to nonvanishing torque induced by the dynamic polarization of the target. To illustrate this point, we assume that the external charge density $\hat{\rho}_{\text{ext}}(\mathbf{R})$ is both highly peaked and appreciable only around point $\mathbf{R}_0=\{\mathbf{r}_0,z_0\}$ in the moving frame, giving rise to a well-defined multipole expansion [35], with total charge $Q=\int d^3\mathbf{R}\hat{\rho}_{\text{ext}}(\mathbf{R})$, and electric dipole with moment $\boldsymbol{\mu}=\int d^3\mathbf{R}(\mathbf{R}-\mathbf{R}_0)\hat{\rho}_{\text{ext}}(\mathbf{R})$. Consequently, one can approximate the structure factor $\mathcal{F}$ by using the Taylor expansion of $f(\mathbf{R};\mathbf{k})$ about $\mathbf{R}_0$, so that

$$\mathcal{F}(\mathbf{k}) \approx \int d^3\mathbf{R}\hat{\rho}_{\text{ext}}(\mathbf{R})[f(\mathbf{R}_0;\mathbf{k})+(\mathbf{R}-\mathbf{R}_0)\cdot\boldsymbol{\nabla}f(\mathbf{R};\mathbf{k})|_{\mathbf{R}=\mathbf{R}_0}] \quad (24)$$

$$=[Q-\boldsymbol{\mu}\cdot(i\mathbf{k}+k\mathbf{e}_z)]f(\mathbf{R}_0;\mathbf{k}), \quad (25)$$

and consequently,

$$|\mathcal{F}(\mathbf{k})|^2 \approx [(Q-k\mu_z)^2+(\boldsymbol{\mu}_\parallel\cdot\mathbf{k})^2]e^{-2kz_0}, \quad (26)$$

with $z_0>0$ being the projectile distance from graphene and μ_z and $\boldsymbol{\mu}_\parallel$, respectively, the components of its dipole moment perpendicular and parallel to graphene. We note that, by setting $Q\neq 0$ and $\boldsymbol{\mu}=\mathbf{0}$ we obtain the point-charge model for fast ions, whereas taking $Q=0$ along with $\boldsymbol{\mu}\neq\mathbf{0}$ gives the point-dipole model suitable for representing polar molecules with permanent electric dipole traveling parallel to graphene at distances greater than, say, 1 Å. Moreover, in this limit of point dipole, the centroid of charge $\mathbf{R}_0$ coincides with the dipole's center of mass. Thus, the assumption of strong localization of the external charge distribution allows the torque on a point dipole around its center of mass to be approximated on the basis of Eq. (23) as $\boldsymbol{\tau}\approx\boldsymbol{\mu}\times\hat{\mathbf{E}}_{\text{ind}}(\mathbf{R}_0)$.

III. RESULTS

We study separately the cases of a point ion and a point dipole. For a point charge Q moving along the x axis with speed v at the distance $z_0>0$ above graphene, the stopping and the image forces are the x and z Cartesian components of the induced force (22) given by, respectively,

$$F_s^{(i)} \equiv \frac{\mathbf{v}\cdot\mathbf{F}_{\text{ind}}}{v} = \frac{Q^2}{2\pi}\int\int dk_x dk_y e^{-2kz_0}\frac{k_x}{k}\,\text{Im}\left[\frac{1}{D(k,k_x v)}\right], \quad (27)$$

$$F_i^{(i)} \equiv -\frac{d\mathcal{E}_{\text{self}}}{dz_0} = \frac{Q^2}{2\pi}\int\int dk_x dk_y e^{-2kz_0}\,\text{Re}\left[\frac{1}{D(k,k_x v)}-1\right], \quad (28)$$

where we have used the symmetry properties of the real and imaginary parts of the function $D(k,\omega)$.

In Figs. 1 and 2 we display the velocity dependencies of the stopping and the image forces on proton ($Q=1$) at distances $z_0=1$ and 3, respectively. Results are shown for three cases: two-fluid model of graphene with (dash-dotted lines) and without (solid lines) SiO_2 substrate (with $\epsilon\approx 3.9$ and $h\approx 4.2$ [8,30]), as well as a one-fluid model for all four valence electrons in graphene without substrate (dashed lines) [36]. One notices effects which are similar to those obtained for proton channeling in carbon nanotubes in analogous situations [26,29,36]. For example, the presence of a substrate is seen to slightly decrease the magnitudes of both forces at high speeds without affecting their low-velocity behavior [29]. On the other hand, the presence of the low-energy, quasiacoustic plasmon in the two-fluid model gives rise to resonant features at low velocities around its "acoustic" speed $v_a\approx 0.71$, which are not seen in the one-fluid model, while the two models give virtually indistinguishable results for both forces at high speeds [26]. In addition, while dynamic thresholds are seen in Figs. 1(a) and 2(a) for stopping forces at the speeds $v\approx 0.7$ (for the two-fluid model) and $v\approx 2$ (for both models), Figs. 1(b) and 2(b) show marked differences between the two models in the values of image forces at low speeds. While this is a consequence of the peculiar features of static screening in 2D within the linearized Thomas-Fermi model [37], we note that our hydrodynamic model of graphene is least reliable at low projectile speeds as it ignores the details of the energy dispersion in the π electron bands of graphene. When this is taken into account, it has been shown recently that the static screening in an intrinsic graphene cannot be treated by a linearized Thomas-Fermi model [38]. Finally, it is worth mentioning that Figs. 1(b) and 2(b) imply that, towards the highest speeds displayed, the effect of the substrate tends to slightly increase the magnitude of the image force. This can be explained by the fact

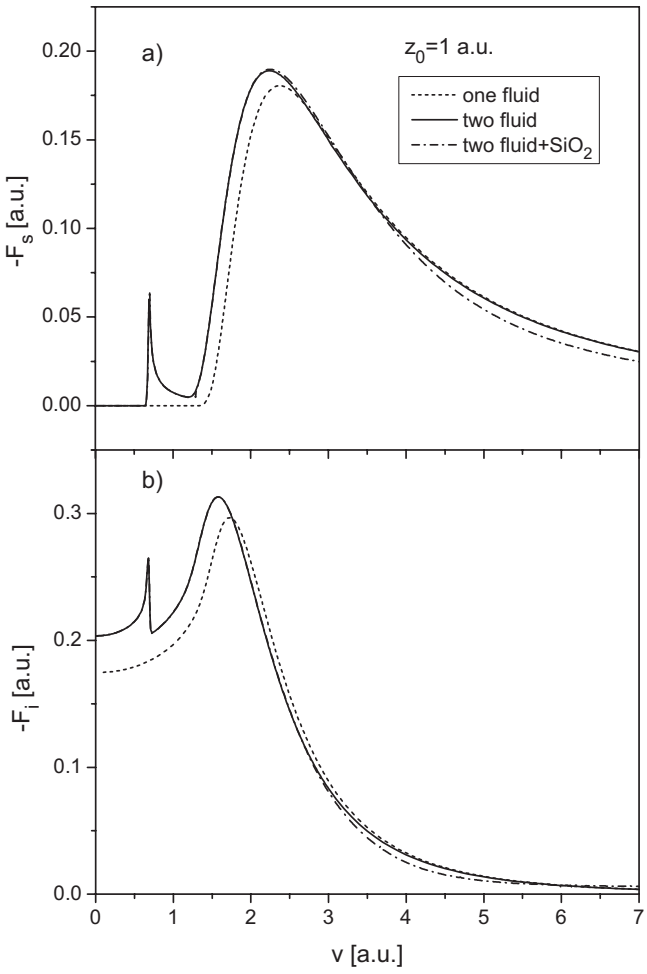

FIG. 1. The dependencies on speed v (in a.u.) of (a) stopping and (b) image forces (in a.u.) on proton moving at distance $z_0=1$ a.u. above graphene in the cases: (solid lines) two-fluid model without substrate, (dashed lines) one-fluid model without substrate, (dash-dotted lines) two-fluid model with SiO_2 substrate (with $\epsilon \approx 3.9$ and $h \approx 4.2$ a.u.).

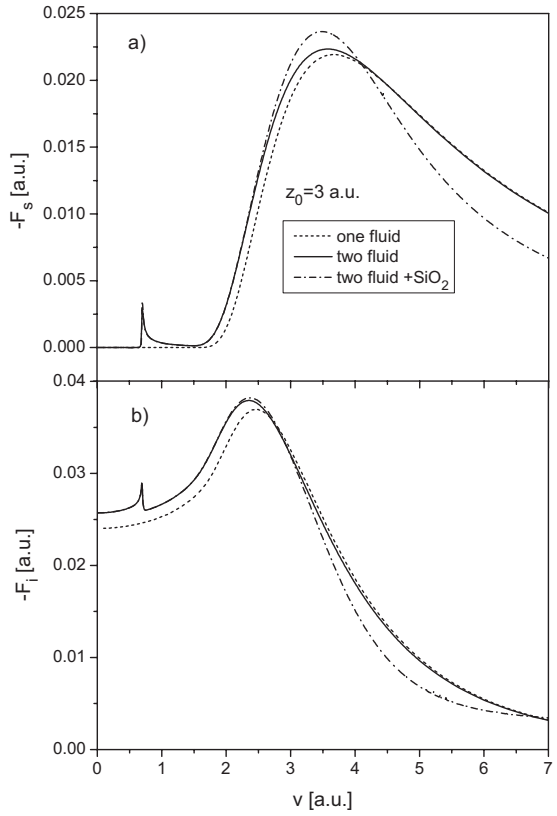

FIG. 2. The dependencies on speed v (in a.u.) of (a) stopping and (b) image forces (in a.u.) on proton moving at distance $z_0=3$ a.u. above graphene in the cases: (solid lines) two-fluid model without substrate, (dashed lines) one-fluid model without substrate, (dash-dotted lines) two-fluid model with SiO_2 substrate (with $\epsilon \approx 3.9$ and $h \approx 4.2$ a.u.).

that the screening ability of graphene is diminished at high frequencies [cf. Eqs. (10) and (11)], so that the image force on the projectile is then simply reduced to the static screening by the substrate.

Figures 1 and 2 also imply a strong decrease in the magnitudes of both the stopping and image forces with increasing distances of proton from graphene, which is further illustrated in Fig. 3 for the two-fluid model without a substrate and for three speeds: $v=1$, 3, and 5. The effects of the substrate are so weak in this parameter range that we only show in Fig. 3 the curves corresponding to speed $v=5$ for the case of graphene above the SiO_2 substrate, described as in Figs. 1 and 2. One notices in Fig. 3 that the decay rates of both stopping and image forces are strongly affected by the proton speed, in accordance with the results found for carbon nanotubes [26,29,36].

For a point dipole moving along the x axis with speed v at the distance $z_0>0$ above graphene, we shall use the angles from spherical coordinates to describe the orientation of its moment, $\boldsymbol{\mu}=\{\mu_x,\mu_y,\mu_z\}\equiv\mu\{\sin\theta\cos\varphi,\sin\theta\sin\varphi,\cos\theta\}$, with the polar angle θ taken relative to the z axis and the azimuthal angle φ relative to the direction of motion, i.e., the x axis. So, the stopping and the image forces on the dipole are, respectively,

$$F_s^{(d)}=\frac{\mu^2}{2\pi}\int\int dk_x dk_y e^{-2kz_0}\frac{k_x}{k}[(k_x\cos\varphi+k_y\sin\varphi)^2\sin^2\theta + k^2\cos^2\theta]\mathrm{Im}\left[\frac{1}{D(k,k_x v)}\right], \tag{29}$$

$$F_i^{(d)}=\frac{\mu^2}{2\pi}\int\int dk_x dk_y e^{-2kz_0}[(k_x\cos\varphi+k_y\sin\varphi)^2\sin^2\theta + k^2\cos^2\theta]\mathrm{Re}\left[\frac{1}{D(k,k_x v)}-1\right]. \tag{30}$$

In Figs. 4 and 5 we consider the case of a point dipole at distance $z_0=3$ having the moment of magnitude $\mu=1$, which is oriented in the xz plane (that is, $\varphi=0$) with its direction relative to the z axis given by the angle θ. Figure 4 shows the velocity dependencies of the stopping and image forces for three orientations: $\theta=0$, 45°, and 90° shown with solid, dashed and dash-dotted lines, respectively, whereas Fig. 5 shows the full dependencies on both the angle θ and speed v.

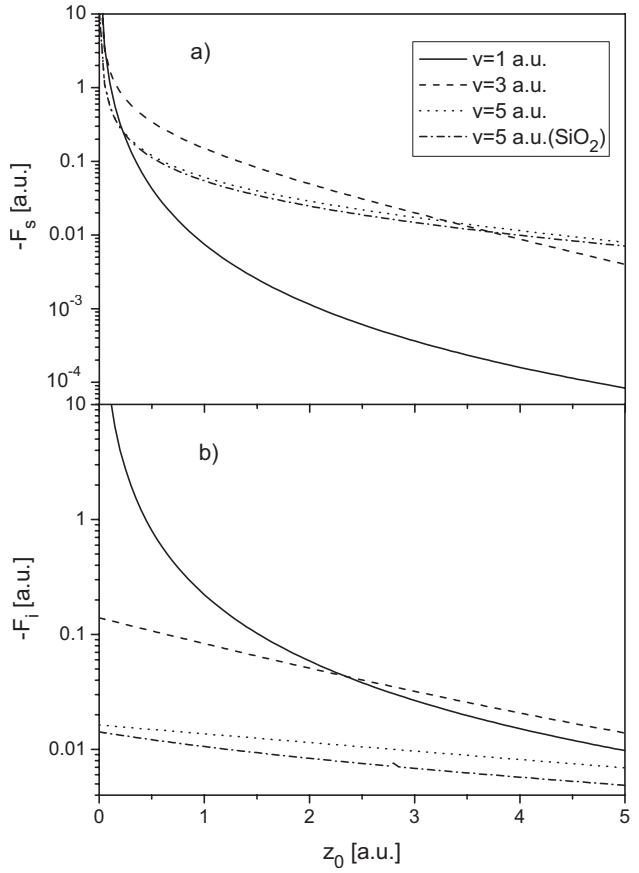

FIG. 3. The dependencies on distance z_0 (in a.u.) of (a) stopping and (b) image forces (in a.u.) on proton moving at speeds $v=1$ a.u. (solid lines), 3 a.u. (dashed lines), and 5 a.u. (dotted lines) for the two-fluid model of graphene without substrate, and at speed $v=5$ a.u. (dash-dotted lines) above graphene with SiO_2 substrate (with $\epsilon \approx 3.9$ and $h \approx 4.2$ a.u.).

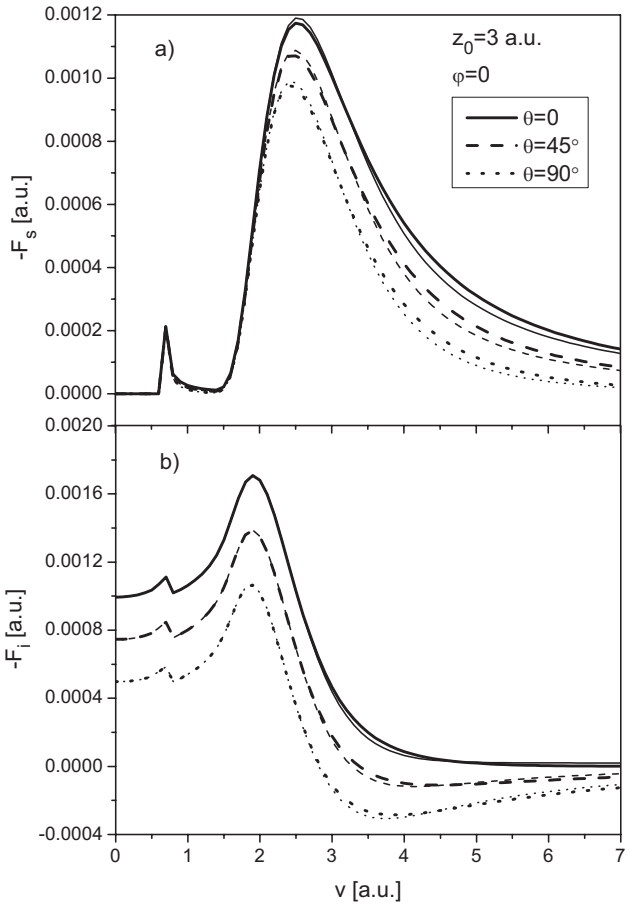

FIG. 4. The dependencies on speed v (in a.u.) of (a) stopping and (b) image forces (in a.u.) on a point dipole moving at distance $z_0=3$ a.u. with the moment $\mu=1$ a.u. orientated in the scattering plane perpendicular to graphene, and with the angle θ relative to the normal to graphene having the values 0° (solid lines), 45° (dashed lines), and 90° (dotted lines). Results are shown for the two-fluid model of graphene without substrate (thick lines) and with SiO_2 substrate (thin lines, with $\epsilon \approx 3.9$ and $h \approx 4.2$ a.u.).

Two cases are displayed in Fig. 4 for the two-fluid models of graphene: no substrate (thick lines), and the SiO_2 substrate (thin lines). One notices similarities with the case of an ion, but with much smaller magnitudes of both forces and relatively weaker effects of the substrate at high speeds. Most importantly, the image force in Fig. 4(b) exhibits an intriguing tendency of becoming repulsive at the intermediate and high speeds for dipole orientations away from the direction perpendicular to graphene. This finding conforms to the results obtained recently for a fast dipole moving over a metal surface [18]. One also notices strong dependencies on angle θ in both the stopping and image forces, which are further revealed in Fig. 5 employing contour plots. It becomes clear from Fig. 5(a) that the stopping force is weakest for dipole orientations in the direction of motion, whereas Fig. 5(b) shows that the dynamic image force becomes most repulsive precisely in those same directions.

Figures 6 and 7 show the dependencies of the stopping and image forces on the angle φ and velocity v for the case of a point dipole at distance $z_0=3$ having the moment of magnitude $\mu=1$, which is oriented along a cone with the (half-) opening angle of $\theta=45°$ relative to the z axis. Figure 6 shows the velocity dependencies of the stopping and image forces for four orientations: $\varphi=0$, 45°, 90° and 135°, shown with solid, dashed, dotted, and dash-dotted lines, respectively, for the case of the two-fluid model of graphene without substrate. The results are similar to those shown in Fig. 4, but with the angular dependencies intricately determined by the dipole speed, as further displayed in Fig. 7, where the periodic φ dependencies of both the stopping and image forces are seen to be shifted to higher angles as the velocity increases.

Finally, the three Cartesian components of torque on a point dipole are

$$\tau_x = \frac{\mu^2}{2\pi} \int\int dk_x dk_y \frac{e^{-2kz_0}}{k} \left\{ -k_x^2 \frac{\sin(2\theta)}{2} \sin\varphi \times \mathrm{Re}\left[\frac{1}{D(k,k_x v)} - 1 \right] + k_x k \frac{\sin(2\varphi)}{2} \sin^2\theta \, \mathrm{Im}\left[\frac{1}{D(k,k_x v)} \right] \right\}, \quad (31)$$

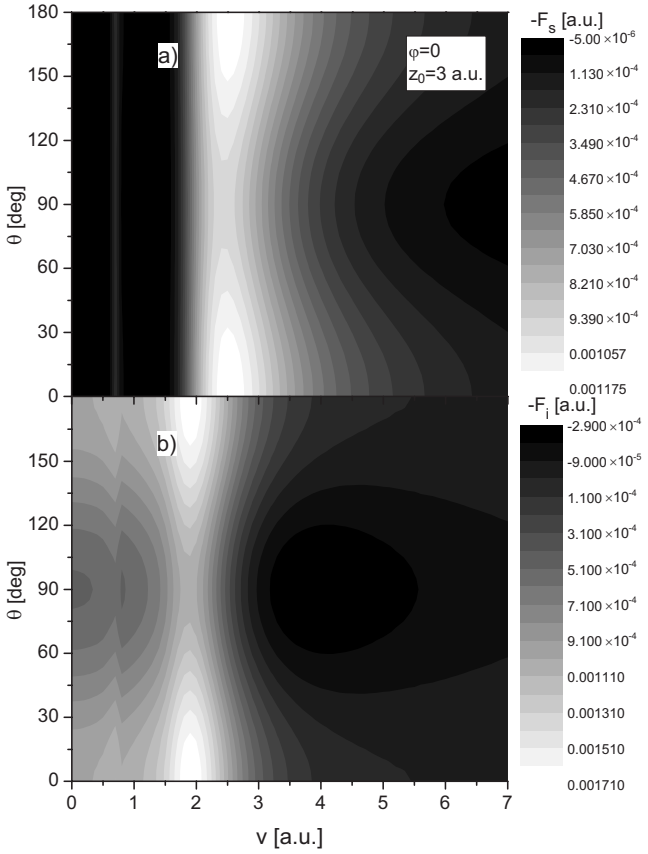

FIG. 5. The dependencies on speed v (in a.u.) and angle θ (in degrees) of (a) stopping and (b) image forces (in a.u.) on a point dipole moving at distance $z_0=3$ a.u. with the moment $\mu=1$ a.u. orientated in the scattering plane perpendicular to graphene, and with the angle θ relative to the normal to graphene. Results are shown for the two-fluid model of graphene without a substrate.

$$\tau_y = \frac{\mu^2}{2\pi}\int\int dk_x dk_y \frac{e^{-2kz_0}}{k}\left\{k_y^2\frac{\sin(2\theta)}{2}\cos\varphi \times \mathrm{Re}\left[\frac{1}{D(k,k_x v)}-1\right] - k_x k(\sin^2\theta\cos^2\varphi+\cos^2\theta) \times \mathrm{Im}\left[\frac{1}{D(k,k_x v)}\right]\right\}, \quad (32)$$

$$\tau_z = \frac{\mu^2}{2\pi}\int\int dk_x dk_y \frac{e^{-2kz_0}}{k}\left\{(k_x^2-k_y^2)\frac{\sin(2\varphi)}{2}\sin^2\theta \times \mathrm{Re}\left[\frac{1}{D(k,k_x v)}-1\right] + k_x k\frac{\sin(2\theta)}{2}\sin\varphi \times \mathrm{Im}\left[\frac{1}{D(k,k_x v)}\right]\right\}. \quad (33)$$

We shall only consider the case of a dipole oriented in the xz plane (that is, for $\varphi=0$) with its direction relative to the z axis given by the angle θ. In that case, the only nonvanishing component of torque is τ_y, describing rotation of the dipole about the y axis passing through its center of mass, and therefore being responsible for dipole's "rolling" over the surface of graphene. In Fig. 8 we show the dependencies of τ_y on both the angle θ and velocity v for a dipole with moment $\mu=1$ moving at the distance $z_0=3$. The effects of substrate are displayed in Fig. 8(a) for the two-fluid model of graphene and for three dipole orientations: $\theta=0$, 45°, and 135°, shown with solid, dashed, and dash-dotted lines, respectively (the case $\theta=90°$ being identical to that of $\theta=0$). One notices the low-velocity resonances around $v_a\approx 0.71$ and a weakening of the torque by the presence of a substrate at high speeds. Interestingly, the change in the sign of torque at low speeds indicates a tendency of the dynamic-polarization forces to align the dipole in the direction of motion, whereas the positive torque values at high speeds indicate that the dipole tends to"roll" along the graphene plane. We note that, although our model is of limited value at low speeds, the conclusion regarding the alignment effect confirms the recent findings for slow polar molecules on solid surfaces [22]. On the other hand, the "rolling" of the dipole at high speeds should be a reliable conclusion coming from our model.

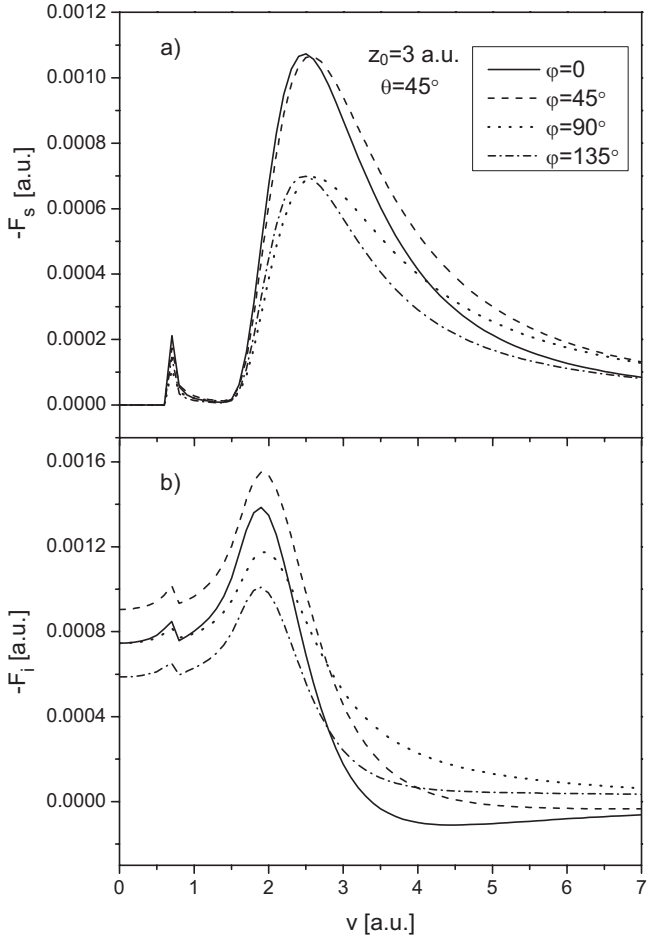

FIG. 6. The dependencies on speed v (in a.u.) of (a) stopping and (b) image forces (in a.u.) on a point dipole moving at distance $z_0=3$ a.u. with the moment $\mu=1$ a.u. orientated with the angle $\theta=45°$ relative to the normal to graphene, and with the angle φ relative to the direction of motion having the values 0° (solid lines), 45° (dashed lines), 90° (dotted lines), and 135° (dash-dotted lines), for the two-fluid model of graphene without a substrate.

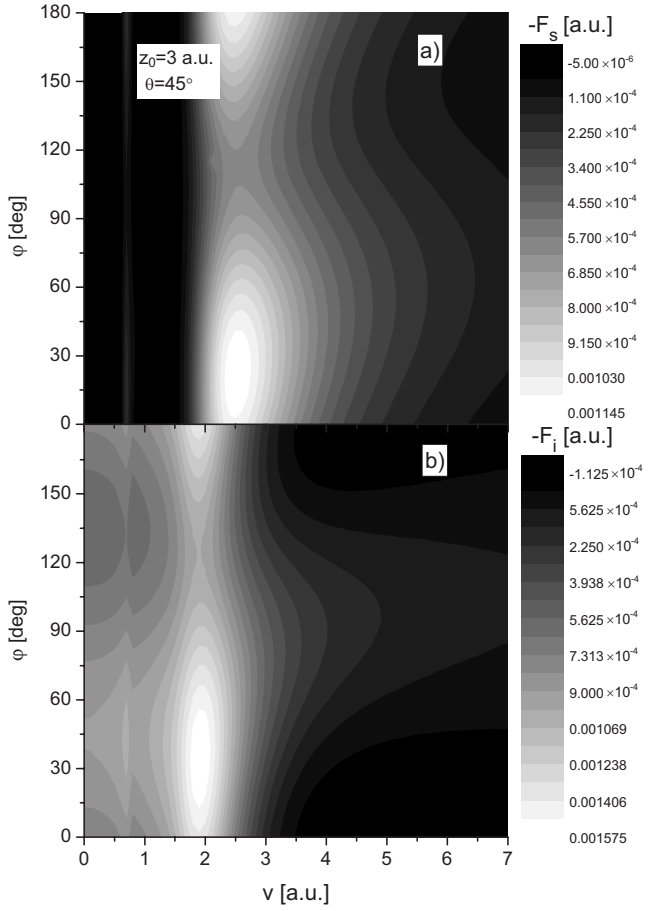

FIG. 7. The dependencies on speed v (in a.u.) and angle φ (in degrees) of (a) stopping and (b) image forces (in a.u.) on a point dipole moving at distance $z_0=3$ a.u. with the moment $\mu=1$ a.u. orientated with the angle $\theta=45°$ relative to the normal to graphene, and with the angle φ relative to the direction of motion, for the two-fluid model of graphene without a substrate.

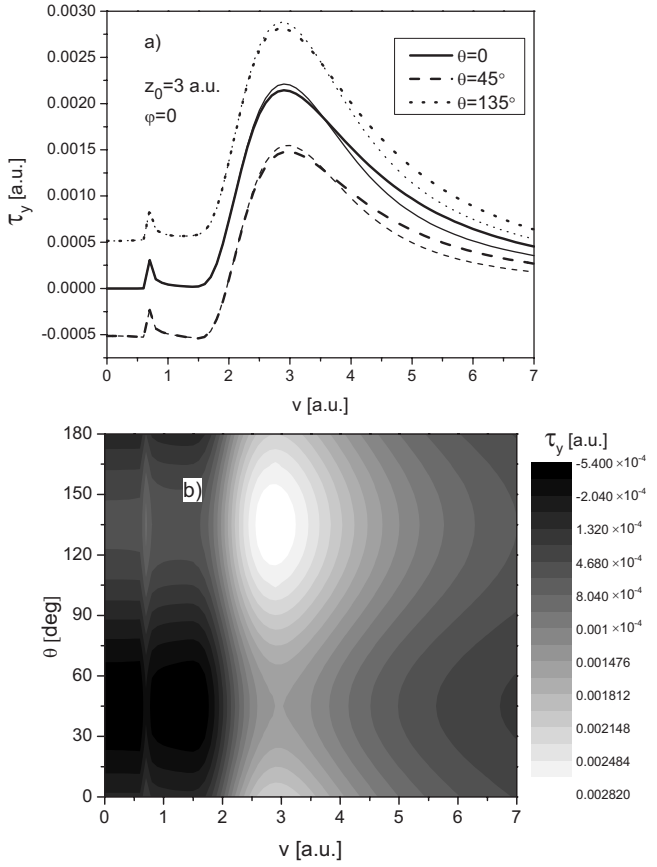

FIG. 8. The dependency on speed v (in a.u.) of the y component of torque (in a.u.) on a point dipole moving at distance $z_0=3$ a.u. with the moment $\mu=1$ a.u. orientated in the scattering plane perpendicular to graphene, and with the angle θ relative to the normal to graphene. (a) Results are shown for $\theta=0°$ and 90° (solid lines), 45° (dashed lines), and 135° (dotted lines), in cases of the two-fluid model of graphene without substrate (thick lines) and with SiO_2 substrate (thin lines, with $\epsilon\approx3.9$ and $h\approx4.2$ a.u.). (b) The dependencies on speed v (in a.u.) and angle θ (in degrees) are shown for the two-fluid model of graphene without substrate.

IV. CONCLUDING REMARKS

We have used a simple 2D, two-fluid model to describe the collective electronic excitations of graphene in response to fast charge distributions moving parallel to it. This model reproduces qualitatively the split of plasmon dispersions into the low-frequency π-electron branch and the high-frequency $\sigma+\pi$-electron branch, which are differently affected by the presence of an insulating substrate. We have calculated both the stopping force and the image force on point ions and point dipoles, as well as the torque acting on point dipoles moving parallel to graphene. The results obtained for the stopping and image forces on point ions are qualitatively similar to those found earlier for ion channeling through carbon nanotubes embedded in dielectric medium [29]. Specifically, the effects of the substrate are found to mostly reduce the high-velocity magnitudes of all calculated quantities, but these effects are relatively weak owing to a large gap between the graphene sheet and substrate, as was recently demonstrated for the SiO_2 substrate [30].

The results obtained for the stopping and image forces on point dipoles are qualitatively similar to those found recently for electric dipoles moving parallel to metal surfaces [18]. Most notably, the image force on dipoles is found to become repulsive at the medium-to-high speeds and for the dipole moments oriented in the direction of motion. In addition, we have presented here the first calculations of torque acting on fast point dipoles about their center of mass moving parallel to a planar nonhomogeneous electron distribution. The torque is found to consist of both the dissipative and conservative parts and is therefore comparable in magnitude to the stopping and image forces on dipole. In the special case of the dipole moment oriented in the scattering plane perpendicular to graphene, the sign of torque implies a strong alignment of the dipole moment in the direction of motion at low speeds, in accord with recent findings for polar molecules at solid surfaces [22]. On the other hand, our finding that the dynamic torque at high speeds seems to give rise to the

dipole rolling over graphene may be further extrapolated to the case of electric dipoles moving parallel to metal surfaces [18].

Although further studies of dynamic interactions of fast charges with graphene are warranted on an expanded parameter space and, particularly, with improved descriptions of the graphene dielectric response, we believe that the model presented here and the results obtained have the merit of an easy tractability and transparency, while providing qualitatively useful implications for a range of future experiments.

ACKNOWLEDGMENTS

This work has been supported by the Ministry of Science, Republic of Serbia. Z.L.M. also acknowledges support by the Natural Sciences and Engineering Research Council of Canada.

[1] K. S. Novoselov, A. K. Gelm, S. V. Morozov, D. Jiang, Y. Zhang, D. V. Dubonos, I. V. Grigorieva, and A. A. Firsov, Science **306**, 666 (2004).
[2] K. S. Novoselov, A. K. Geim, S. V. Morozov, D. Jiang, M. I. Katsnelson, I. V. Grigorieva, S. V. Dubonos, and A. A. Firsov, Nature (London) **438**, 197 (2005).
[3] M. I. Katsnelson, Mater. Today **10**, 20 (2007).
[4] W. L. Barnes, A. Dereux, and T. W. Ebbesen, Nature (London) **424**, 824 (2003).
[5] O. Vafek, Phys. Rev. Lett. **97**, 266406 (2006).
[6] E. H. Hwang and S. Das Sarma, Phys. Rev. B **75**, 205418 (2007).
[7] V. Ryzhii, A. Satou, and T. Otsuji, J. Appl. Phys. **101**, 024509 (2007).
[8] G. Bertoni, L. Calmels, A. Altibelli, and V. Serin, Phys. Rev. B **71**, 075402 (2005).
[9] A. G. Marinopoulos, L. Wirtz, A. Marini, V. Olevano, A. Rubio, and L. Reining, Appl. Phys. A: Mater. Sci. Process. **78**, 1157 (2004).
[10] M. Dapor, L. Calliari, and M. Filippi, Nucl. Instrum. Methods Phys. Res. B **255**, 276 (2007).
[11] G. Ramos and B. M. U. Scherzer, Nucl. Instrum. Methods Phys. Res. B **85**, 479 (1995); **174**, 329 (2001).
[12] E. Yagi, T. Iwata, T. Urai, and K. Ogiwara, J. Nucl. Mater. **334**, 9 (2004).
[13] S. Cernusca, M. Fürsatz, H. P. Winter, and F. Aumayr, Europhys. Lett. **70**, 768 (2005).
[14] T. Kaneko, H. Kudo, S. Tomita, and R. Uchiyama, J. Phys. Soc. Jpn. **75**, 034717 (2006).
[15] H. Winter, Phys. Rep. **367**, 387 (2002).
[16] K. Tökési, X.-M. Tong, C. Lemell, and J. Burgdörfer, Phys. Rev. A **72**, 022901 (2005).
[17] A. S. El-Said, W. Meissl, M. C. Simon, J. R. Crespo López-Urrutia, I. C. Gebeshuber, M. Lang, HP. Winter, J. Ullrich, and F. Aumayr, Nucl. Instrum. Methods Phys. Res. B **256**, 346 (2007).
[18] I. Villó-Pérez, I. Abril, R. Garcia-Molina, and N. R. Arista, Phys. Rev. A **71**, 052902 (2005).
[19] N. R. Arista, Phys. Rev. A **64**, 032901 (2001).
[20] R. Díez Muiño and A. Salin, Phys. Rev. B **62**, 5207 (2000).
[21] A. Vernov and W. Steele, Langmuir **8**, 155 (1992).
[22] S. K. Sekatskii, Phys. Rev. A **67**, 022901 (2003).
[23] Y.-H. Song, Y.-N. Wang, and Z. L. Mišković, Phys. Rev. A **72**, 012903 (2005).
[24] A. L. Fetter, Ann. Phys. **81**, 367 (1973).
[25] G. Barton and C. Eberlein., J. Chem. Phys. **95**, 1512 (1991).
[26] D. J. Mowbray, Z. L. Mišković, F. O. Goodman, and Y.-N. Wang, Phys. Rev. B **70**, 195418 (2004).
[27] G. Gumbs and A. Balassis, Phys. Rev. B **71**, 235410 (2005).
[28] E. Prodan, C. Radloff, N. J. Halas, and P. Nordlander, Science **302**, 419 (2003).
[29] D. J. Mowbray, Z. L. Mišković, and F. O. Goodman, Phys. Rev. B **74**, 195435 (2006).
[30] M. Ishigami, J. H. Chen, W. G. Cullen, M. S. Fuhrer, and E. D. Williams, Nano Lett. **7**, 1643 (2007).
[31] V. M. Silkin, J. M. Pitarke, E. V. Chulkov, and P. M. Echenique, Phys. Rev. B **72**, 115435 (2005).
[32] T. P. Doerr and Y. K. Yu, Am. J. Phys. **72**, 190 (2004).
[33] B. P. van Zyl and E. Zaremba, Phys. Rev. B **59**, 2079 (1999).
[34] R. G. Parr and W. Yang, *Density-Functional Theory of Atoms and Molecules* (Oxford University Press, New York, 1989).
[35] J. D. Jackson, *Classical Electrodynamics*, 3rd ed. (Wiley, New York, 1999).
[36] Y.-N. Wang and Z. L. Mišković, Phys. Rev. A **69**, 022901 (2004).
[37] A. P. Favaro, K. Capelle, and J. V. Batista Ferreira, Phys. Rev. B **73**, 045133 (2006).
[38] M. I. Katsnelson, Phys. Rev. B **74**, 201401(R) (2006).